Carbon coatings on silicon carbide by reaction with chlorine-containing gases

Yury G. Gogotsi,*[a] In-Deok Jeon[b] and Michael J. McNallan[b]

[a]*University of Illinois at Chicago, Department of Mechanical Engineering, 842 West Taylor St. Chicago, IL60607, USA*
[b]*University of Illinois at Chicago, Department of Civil and Material Engineering, 842 West Taylor St. Chicago, IL60607, USA*

Carbon films have been produced on the surface of β-SiC particles by reaction with $Ar–Cl_2$ and $Ar–Cl_2–H_2$ gas mixtures at atmospheric pressure and temperatures of 600–1000 °C. The structure and composition of the carbon films have been investigated using XRD, SEM, EDS, TEM, FTIR and Raman spectroscopy. BET and TG were also used for measuring the amount of carbon formed in the reaction. Uniform nanoporous carbon films with surface area exceeding 1000 $m^2\ g^{-1}$ were obtained by reactions with $Ar–Cl_2$ gas at 600–1000 °C. Based on Raman spectroscopy and electron diffraction data, these films were identified as nanocrystalline graphite. An addition of hydrogen to the gas mixtures results in the etching of graphitic carbon. Traces of diamond were found along with amorphous carbon after treatment in $Ar–Cl_2–H_2$ gas mixtures at temperatures above 900 °C.

Introduction

Recently, formation of carbon by hydrothermal corrosion of SiC and other carbides at 300–800 °C has been found.[1] The synthesis of carbon coatings on the surface of carbides by hydrothermal leaching was also reported.[2] The formation of both graphitic and tetrahedral carbon on the surface of SiC by hydrothermal methods has also been observed.[3–5] However, hydrothermal treatment can only be applied to carbides that form soluble or volatile hydroxides, such as $Si(OH)_4$. Even for SiC, co-deposition of silica can occur during the treatment.[2–4] Extraction of metals from carbides by halogens (F_2, Cl_2, Br_2 and I_2) or their compounds (HF, CCl_4, $CHCl_3$, *etc.*) can also lead to the formation of free carbon which may have a similar structure to that of the hydrothermal carbon. This method is more versatile because it can be used to obtain carbon from various carbides, since most of metals form volatile halides (*e.g.*, $TiCl_4$, TiI_4, *etc.*), but do not form soluble or volatile oxides. For SiC, it has been reported that the Si-component is preferentially attacked and a carbon-rich layer builds up in the reaction with chlorine or fluorine-containing gases.[6–8] However, there is no published information about the structure and properties of carbon films produced by this method. This carbon formation was observed primarily by researchers studying corrosion or etching of semiconductor materials so the properties of the carbon residue were not of importance. Under some conditions, the presence of halogens may favor diamond formation. Grannen and Chang[9] were able to form a diamond deposit from fluorocarbon gases in a microwave plasma on β-SiC and WC without diamond pretreatment of the substrate. Halogenated hydrocarbons can serve as precursors for both CVD[9] and hydrothermal[10] synthesis of diamond.

Here, we present the results of the treatment of a β-SiC powder with chlorine-containing gases and thermodynamic simulations of possible reactions.

Thermodynamic study

The interaction of SiC with chlorine–oxygen gas mixtures has been previously studied.[11–13] Here, thermodynamic analyses of the reaction products in the system β-SiC/chlorine-containing gases have been conducted in the temperature range 300–1300 °C using a Gibbs energy minimization program. The HSC program developed by Outokumpu Research Oy, Finland at the University of Illinois and Chemsage-3.11 program (GTT Technologies, Germany) at the University of Tübingen were used. The calculations were made in the temperature range from 300 to 1300 °C in 50 °C increments for the following systems:

(1) $SiC + Cl_2(g)$, at 1 atm;
(2) $SiC + Cl_2(g) + H_2(g)$, at 1, 100 and 1000 atm; and
(3) $SiC + 0.9\ Cl_2(g) + H_2(g) + 0.1\ O_2$, at 1 atm.

Thus, the effects of temperature, pressure, $H_2:Cl_2$ ratio and oxygen contamination on the composition of equilibrium reaction products have been studied. The effect of the presence of Ar was also investigated in this simulation.

The hypotheses necessary to carry out the thermodynamic calculations concern the choice of the gas and solid phases and the choice of thermodynamic data. The calculations were done for a closed system with constant total pressure and ideal gases (activity coefficients are equal to unity). More than 60 possible species were taken into account.

The method used for thermodynamic calculations assumes that equilibrium conditions are reached between the gas phase and the solid at the reaction surface. However, kinetic limitations lead to relatively low corrosion rates of carbide samples at temperatures below 400 °C. The calculations have been done for a closed system. However, the experiments were performed in an open system with gases flowing through a tube reactor. Thus, the calculated equilibrium composition was not always reached under the conditions of the experiments. Therefore, comparison of the results of the thermodynamic calculations with the experimental data must be performed with account of the possible differences between the equilibrium and non-equilibrium conditions.

Materials and Experimental procedure

The β-SiC powder used in this experiment (Johnson Matthey, MA) is of 99.8% purity with 1 μm particle size. The X-ray diffraction (XRD) pattern of the as-received powder shows typical β-SiC peaks. The Raman spectrum displays a strong Raman band at 784 cm^{-1} due to transversal optical (TO) phonons of β-SiC and another weak band at *ca.* 1500 cm^{-1} which can be ascribed to C—C bonds in SiC.[14] The shape of the spectrum is typical for disordered fine grain β-SiC. The spectrum of the as-received powder also contains some free carbon as indicated by two bands at 1570 and 1324 cm^{-1}. The former is referred to as the G mode and attributed to doubly degenerated E_{2g} in-plane stretching mode of graphite.[15] The latter originates from phonon scattering from the boundary of

the graphite Brilliouin zone and is referred to as the D mode of graphite. It is known to be active in small graphite crystallites, as the grain size becomes of the same order as the incident phonon wavevector. Its position depends on the excitation wavelength and is observed at 1350–1355 cm^{-1} for the 514.5 nm excitation line of an Ar laser and at *ca.* 1325 cm^{-1} for the 632.8 nm line of the He–Ne laser. Both TEM and micro-Raman studies demonstrated the presence of traces of carbon as inclusions with size <1 μm.

Experiments to produce carbon by reaction with chlorine were performed in the apparatus shown schematically in Fig. 1. The gases H_2 and Cl_2, supplied in premixed cylinders with argon, were purified to remove H_2O and CO_2 by passage through packed columns of anhydrous $CaSO_4$ and Ascarite and mixed in a packed column. The gas flow rate was 1.5 cm^3 s^{-1} in the reaction tube. Powdered β-SiC was contained in a platinum foil crucible suspended in the hot zone of the furnace. Experiments were continued for 5–72 h depending on the reactivity of the environment. Gas mixtures containing 2–3.5% Cl_2 and 0–2% H_2 at temperatures from 500 to 1000 °C were used. Although argon was always present as the main component of the gas mixture, it was an inert addition. Therefore, when describing the gas composition in the text, we shall ignore the presence of argon and mention only H_2 and Cl_2 contents in the mixture.

After treatment with gases, the powders were investigated by XRD, scanning electron microscopy (SEM), X-ray energy dispersive spectroscopy (EDS), FTIR spectroscopy, transmission electron microscopy (TEM) and Raman spectroscopy. The use of all of the above methods to analyze the reaction products in the Si–C–O system and the problems encountered in doing so were discussed in detail by Gogotsi *et al.*[16]

A Siemens-5000 X-ray diffractometer with Cu-Kα radiation was used for X-ray diffraction analysis. A JEM 35C (JEOL, Japan) scanning electron microscope was used for SEM and EDS analyses.

The Raman analyses were conducted using a LabRam II micro-Raman spectrometer (Dilor, France) at the University of Tübingen, Germany. An Ar ion laser at a wavelength of 514.5 nm and a He–Ne laser at a wavelength of 632.8 nm were used for Raman analysis of the powders. The powders were placed on an aluminium foil or a glass plate for micro-Raman measurements. The spectra were obtained using magnifications of ×1000 (×100 objective lens) and ×100 (×10 objective lens). The wavenumber range from 200 to 1800 cm^{-1} was covered. All phases which exist in the Si–C–O system have Raman bands in this range. Spectra from selected samples were recorded in the range from 50 to 7000 cm^{-1}. At least ten measurements were done on each powder to obtain reliable and reproducible spectra.

FTIR studies were conducted using a Bruker spectrometer at the University of Tübingen. Samples for FTIR spectroscopy were prepared by mixing the powders with KBr and pressing to form a pellet. The volume-filling factor of the powder was 0.005. FTIR absorption spectra were measured in the frequency range 400–4000 cm^{-1}.

Three samples after treatments under different conditions were chosen for TEM analysis. The powders were observed in a JEM 200CX transmission electron microscope operating at 200 kV. This analysis was carried out at the center for Materials Research, University of Oslo. The particle types were identified by selected area diffraction (SAD) patterns. TEM samples were prepared by mixing powders with ethanol in an ultrasonic bath, followed by filtration of the particles which were collected on a supporting copper grid covered with a perforated carbon film.

After the treatment of the powder, the surface area was measured by the BET method. To measure the total content of carbon formed the treated samples were oxidized at 750 °C in air at atmospheric pressure. The mass change after oxidation was measured.

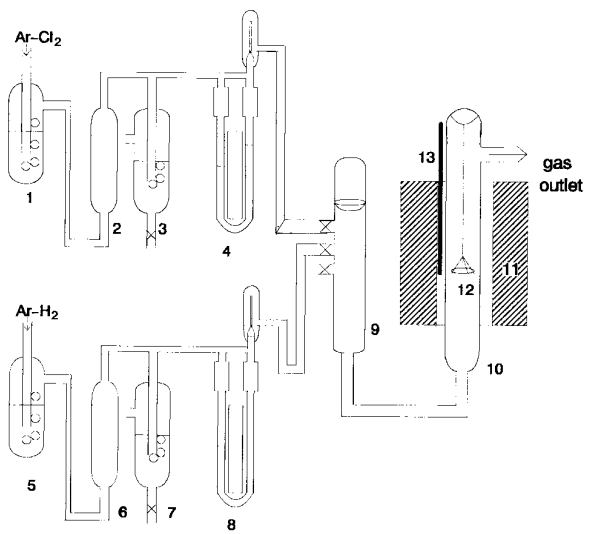

Fig. 1 Schematic diagram of the apparatus for etching in chlorine-containing gases. 1,3: H_2SO_4; 2,6: dessicant; 4,8: capillary flowmeter; 5,7: dibutyl phthalate; 9: mixing column; 10: quartz reaction tube; 11: resistance furnace; 12: Pt dish and quartz wire; 13: thermocouple.

Results

Thermodynamic simulations

From the results shown in Fig. 2–5, carbon formation is expected in reactions with both Cl_2 and Cl_2–H_2. In the system of SiC/Cl_2, the reaction

$$SiC\ (g) + 2\ Cl_2\ (g) = CCl_4\ (g) + Si\ (s) \quad (1)$$

is rather slow. The reaction

$$SiC + 2\ Cl_2 = SiCl_4\ (g) + C\ (s) \quad (2)$$

is most favorable thermodynamically and at higher temperature (above 900 °C), the thermodynamic probability of the reaction

$$SiC\ (s) + 2/3\ Cl_2 = SiCl_3\ (g) + C\ (s) \quad (3)$$

increases. The probability of CCl_4 formation decreases with

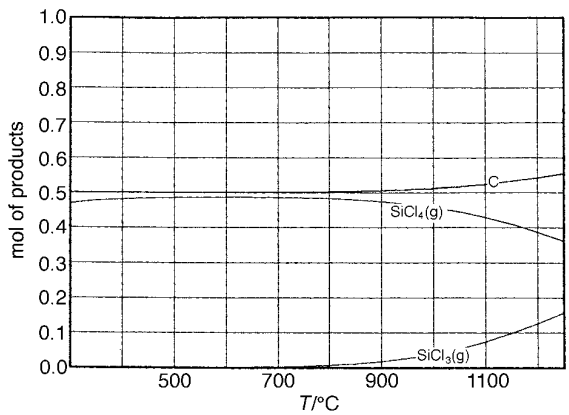

Fig. 2 Equilibrium reaction products, calculated by HSC for $P = 1$ atm and molar ratio $Cl_2 : SiC = 1 : 1$

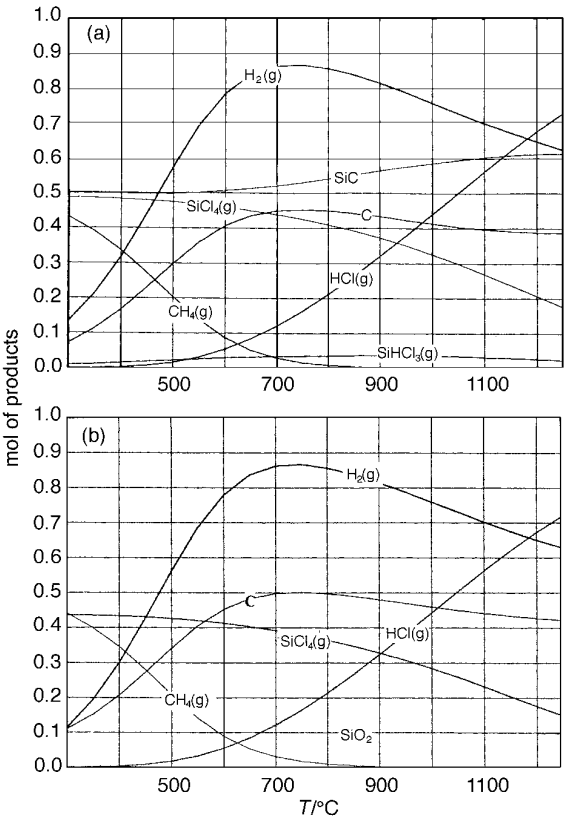

Fig. 3 Equilibrium compositions calculated by HSC for $P=1$ atm: (a) molar ratio $Cl_2:H_2:SiC=1:1:1$ and (b) molar ratio $Cl_2:H_2:O_2:SiC=0.9:1:0.1:1$

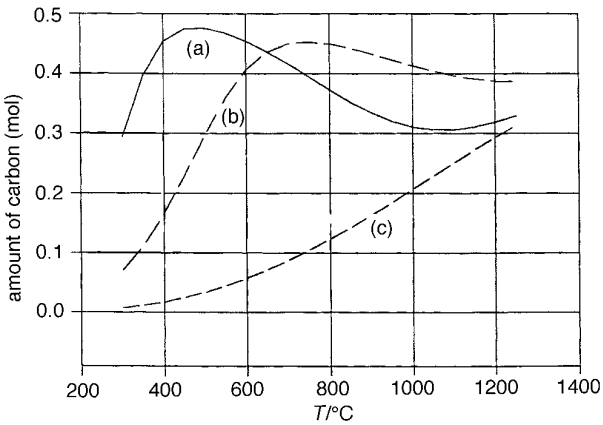

Fig. 4 Simulated effect of pressure on carbon formation in the $SiC–Cl_2–H_2$ system for the molar ratio $Cl_2:H_2:SiC=1:1:1$: (a) $P=$ 0.01 bar, (b) $P=1.0$ bar, (c) $P=1.0$ kbar

increasing temperature. When hydrogen is added to the system, HCl is formed by the reaction

$$H_2\,(g)+Cl_2\,(g)=2HCl\,(g) \quad (4)$$

It can react with SiC as follows.

$$SiC\,(s)+4HCl\,(g)=SiCl_4\,(g)+C\,(s)+2\,H_2\,(g) \quad (5)$$

$$SiC\,(s)+3HCl\,(g)=SiHCl_3\,(g)+C\,(s)+H_2\,(g) \quad (6)$$

$$C\,(s)+2H_2\,(g)=CH_4\,(g) \quad (7)$$

Additionally, if oxygen impurities are present, SiO (g), CO (g), CO_2 (g) and SiO_2 (s) could be formed.

In the $SiC/Cl_2–H_2$ system, the predicted amount of carbon is somewhat lower than that in the SiC/Cl_2 system and it

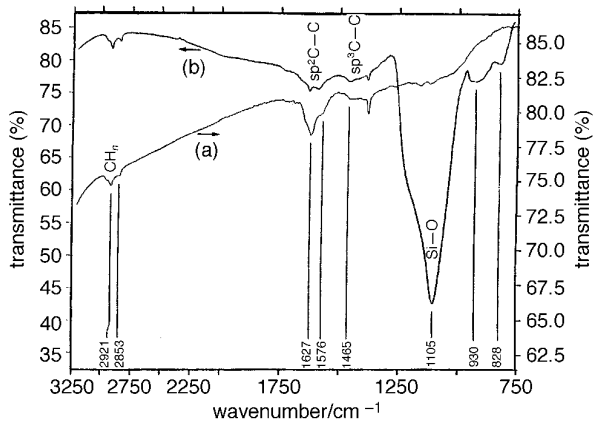

Fig. 5 FTIR spectra of β-SiC powders treated in (a) Ar–3.5% Cl_2 at 1000 °C for 20 h and (b) Ar–2.6% Cl_2–1.3% H_2 at 950 °C for 72 h

decreases with increasing $H_2:Cl_2$ ratio. The yield of methane, which is unstable at high temperatures, decreases with increasing temperature so that the carbon yield increases. The carbon and hydrogen yields pass through a maximum, and at higher temperatures, the amount of HCl increases rapidly and that of carbon decreases. The maximum hydrogen and carbon contents in the reactor are obtained around 800 °C in the $SiC/Cl_2–H_2$ system as shown in Fig. 3.

At higher pressure, the temperature at which the carbon content in the reaction products is maximized, increases as shown in Fig. 4. This is due to the increasing stability of methane and other hydrocarbon species formed at high pressure. A small addition of oxygen leads to the formation of silica (quartz), but does not affect the relative amounts of other species in the system as shown in Fig. 3(b).

When argon is present in the gas mixture, the temperature that corresponds to the maximum hydrogen and carbon contents in the reactor decreases to around 500 °C. This is similar to the effect of decreasing total pressure.

Experimental studies

The chlorination kinetics of SiC has been described in a recent publication[17] and will not be discussed here. A mass loss was observed in agreement with the thermodynamic predictions.

XRD. After a treatment in 3.5% Cl_2 at 600 °C, the XRD pattern was much the same as that of the as-received powder. After reactions with 3.5% Cl_2–Ar at 800 and 1000 °C the intensity of β-SiC reflections diminished and disappeared with increasing reaction time. However, no other peaks were detected. In the sample treated with $Cl_2–H_2$ mixed gases, only β-SiC Bragg reflections were detected without any other signals present.

SEM and EDS. For the experiment with 3.5% Cl_2 at 1000 °C, EDS showed a substantial increase in the C : Si ratio compared to the untreated powder. However, the amount of oxygen was below the sensitivity of the method. For treatment with 2% Cl_2–2% H_2 at 1000 °C, the intensity of the Si peak was the same as that of the untreated powder. The intensity of carbon and oxygen peaks increased slightly compared to the untreated powder. From the data of XRD and EDS, we expect that the treatment in Cl_2 results in the formation of amorphous carbon. The carbon yield is higher at higher temperatures. However, in the 2% Cl_2–2% H_2 atmosphere, the reaction rate is very low. This was also confirmed through TG measurements.[17]

FTIR spectroscopy. IR spectroscopy is useful for analysis of Si—O and C—H bonding, but its sensitivity to free carbon is

low. Pure diamond does not have any IR-active modes. IR bands corresponding to C=C bonds are weak compared to those of Si—C or Si—O bonds. Therefore, this analysis was primarily used to detect silica in the samples.

Silica was detected in all samples treated in Cl_2–H_2 as shown in Fig. 5. The silica band at *ca.* 1100 cm^{-1} became much stronger compared to that of as-received powder and it also increased as the Cl_2:H_2 ratio increased. However, silica was not found in the powders treated with 3.5% Cl_2 at 800 or 1000 °C. The results are in agreement with the EDS data. Although oxygen was not detected in the particles treated at 800 and 1000 °C by EDS and FTIR spectroscopy, in this case, silica was found around the Pt dish or on the sample suspension wire. At temperatures above 800 °C, after Si is etched from SiC by Cl_2, the $SiCl_4$(g) reacts with O_2(g) to form SiO_2 or SiO. Silicon oxychloride compounds (Si_2OCl_6 and Si_3OCl_8) can also be formed during the high-temperature reaction of SiC with Cl_2–O_2 mixtures.[18] Besides silica, sp^2 carbon (bands at *ca.* 1580–1630 cm^{-1}) was detected in powders treated with Cl_2–H_2 at 950 °C and with 3.5% Cl_2 at 1000 °C. The amplitude of the band was much higher in the latter case, as shown in Fig. 5. The former one shows a similar amplitude of the carbon band to that of untreated powder. Bands corresponding to CH_n vibrations were observed in the wavenumber range 2850–3000 cm^{-1}.

Raman spectroscopy. In the spectra of the powders treated in 3.5% Cl_2 at 600 and 1000 °C, bands of disordered graphite were observed as shown in Fig. 6 along with β-SiC and amorphous silica. Here, the relative intensity of the G band of graphite compared to the D band increases with temperature. This implies that the size of the graphite crystallites increases as temperature increases. For evaluation of the graphite crystal size (in-plane dimension) L_a we used the equation,[20]

$$L_a = 4.4\ (I_D/I_G)^{-1} \quad (8)$$

where L_a is the size of graphite crystallites in nm and I_D and I_G are intensities of D and G bands of graphite, respectively. The results are summarized in Table 1. The average size of graphite crystallites formed in the treatment with 3.5% Cl_2 was estimated as 2–4 nm.

While a strong SiC band was observed in the spectrum of the powder treated at 600 °C, in the powder treated at higher temperatures (1000 °C), the SiC band disappeared and only carbon bands were found, as shown in Fig. 6(b). From this, we can conclude that the carbon yield increases with temperature. These results are in agreement with XRD and EDS data.

Fig. 7 shows the Raman spectra of the powder treated in Cl_2–H_2 mixture gases. Overall in these Raman spectra, a strong SiC band was observed and less carbon was present in the powders. However, the average intensity of the carbon bands increased compared to that in the starting material and thus, some carbon was formed during this treatment.

In experiments with 2%Cl_2–2%H_2 at 800 °C [Fig. 7(a)], a broad band appeared, probably due to the superposition of the D band of graphite, the G band, and a band at 1500 cm^{-1}. The latter has been observed in carbon-rich SiC:H alloy or SiC.[15]

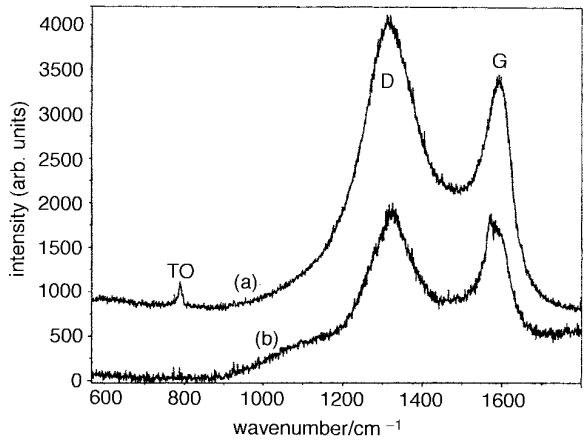

Fig. 6 Typical Raman spectra (excitation line 632.8 nm) of β-SiC powders treated in Ar–3.5% Cl_2 at (a) 600 °C for 27 h and (b) 1000 °C for 20 h

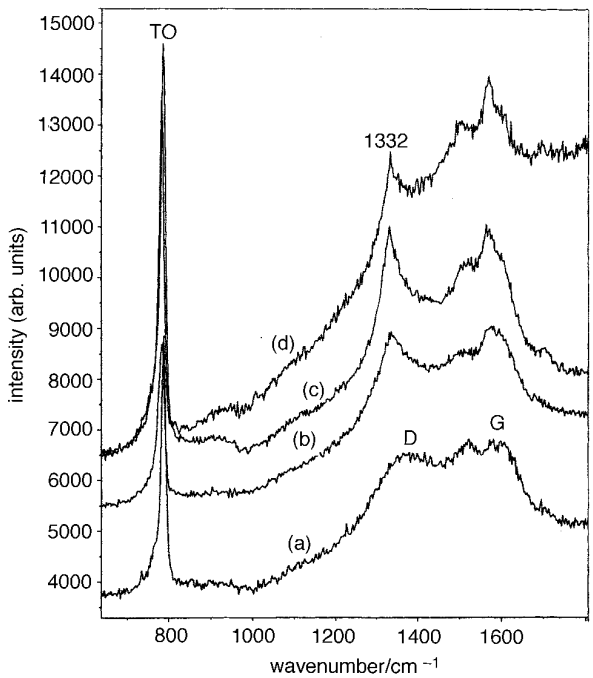

Fig. 7 Typical Raman spectra (excitation line 514.5 nm) of β-SiC powders treated in (a) Ar–2% Cl_2–2% H_2 at 800 °C for 24 h, (b) Ar–2% Cl_2–2% H_2 at 950 °C for 24 h and (c), (d) Ar–2.6% Cl_2–1.3% H_2 at 800 °C for 24 h (two examples)

Fig. 7(b) shows the Raman spectrum of the powder treated in 2%Cl_2–2%H_2 at 950 °C. It is very similar with the spectrum of amorphous carbon, but the D band is shifted closer to the diamond region (1333 cm^{-1}); it is becoming sharp and the band at 1500 cm^{-1} is stronger. An increasing Cl_2–H_2 ratio results in

Table 1 Surface area and size of graphite crystallites in SiC powders treated in Ar–Cl_2 and Cl_2–H_2 gases

experimental conditions						
gas	T/°C	t/h	S^a/m^2 g^{-1}	mass% C	$S_C{}^b$/m^2 g^{-1}	L_a/nm
3.5% Cl_2–Ar	600	27	47.8	8	400	2.0–2.5
3.5% Cl_2–Ar	600	48	140.0	11	1163	2.4–2.6
3.5% Cl_2–Ar	1000	20	989.6	98	1010	2.0–4.5
2% Cl_2–2% H_2–Ar	1000	72	11.5	<5%	10	1.0–4.5
as-received β-SiC			13.6	<3%		2.0

^aS = Specific surface area of powder. ^bS_C = Calculated surface area of carbon.

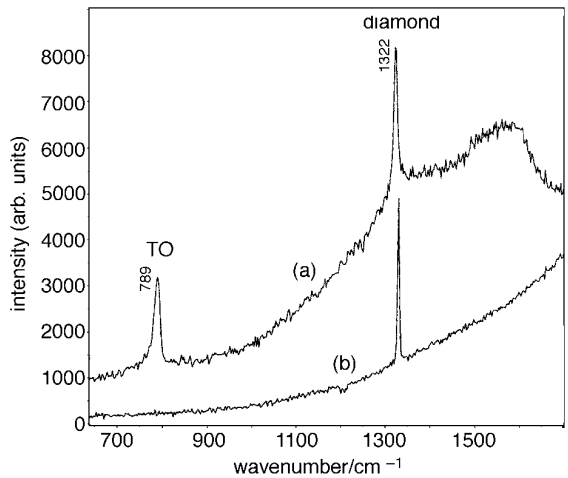

Fig. 8 Typical Raman spectra (excitation line 514.5 nm) of β-SiC powders treated in Ar–2.6% Cl_2–1.3% H_2 at 950 °C for 24 h, (a) regular region and (b) diamond region

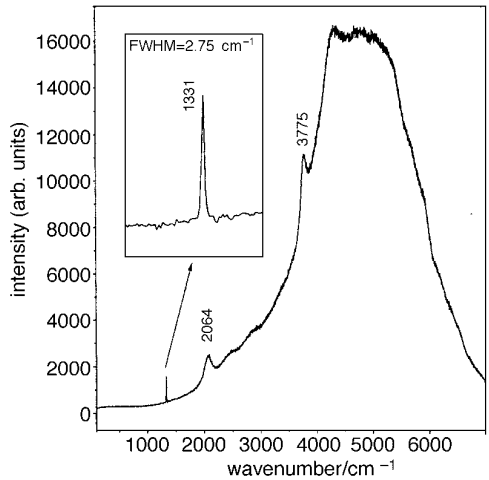

Fig. 9 Full Raman spectrum (excitation line 514.5 nm) of the diamond region in the β-SiC powder treated in Ar–2.6% Cl_2–1.3% H_2 at 950 °C for 24 h

even stronger and sharper bands at *ca.* 1332 cm^{-1}. Two typical examples are shown in Fig. 7(c) and (d).

Fig. 8(a)–(b) show the Raman spectra of the powder treated in 2.6%Cl_2–1.3%H_2 at 950 °C. Here, the sharp band at *ca.* 1330 cm^{-1} cannot be ascribed to D band of graphite and is obviously a diamond band. Therefore, well crystallized diamond must be present in this sample. The D band of graphite can overlap with the diamond band [Fig. 8(a)]. At the same time, pure diamond has been found in several points of this sample as shown in Fig. 8(b). The downshift of the diamond band is probably due to a small grain size and/or laser heating.[21] The amount of diamond in the powder is small (probably $<1\%$), but diamond regions are clearly visible under a microscope. Some of them produce a Raman band of diamond which is not accompanied by SiC or graphite peaks [Fig. 8(b)]. This means that the size of these regions is of the order of a few micrometers; however, the crystals are probably smaller than 1 micrometer. No well shaped crystals have been observed by optical microscopy. It is important to note that regions of pure diamond produce a narrow band (full width at half maximum is 3–4 cm^{-1}) centered at *ca.* 1332 cm^{-1}, while mixed SiC, diamond and graphite regions produce a broad band (width >7 cm^{-1}) shifted to lower frequencies. This means that the quality (size, perfection) of diamond is higher in the regions of pure diamond. Diamond regions also produced a strong luminescence peak at *ca.* 4500 cm^{-1} as shown in Fig. 9. A similar luminescence has been observed for CVD diamond and can be attributed to crystal defects introduced in the growth process. The small size and content of diamond are confirmed by the fact that the diamond band disappeared after homogenization of the powder. When uniformly distributed, the diamond signal was below the sensitivity of the analysis. Fig. 10 shows the Raman spectrum of the powder treated in 2% Cl_2–2% H_2 at 1000 °C. Here, a broad band in the region of diamond phonon (1332 cm^{-1}) and an extremely weak G band of graphite were observed. A very weak band at *ca.* 1130 cm^{-1} may correspond to amorphous diamond.[15] Very similar spectra were obtained from the powder treated with 2.6% Cl_2–1.3% H_2 at 950 °C. A broad band at 1140 cm^{-1} which is ascribed to amorphous diamond was observed along with another broad band at around 1330 cm^{-1}. Similar spectra were also obtained from nanocrystalline CVD diamond.[22]

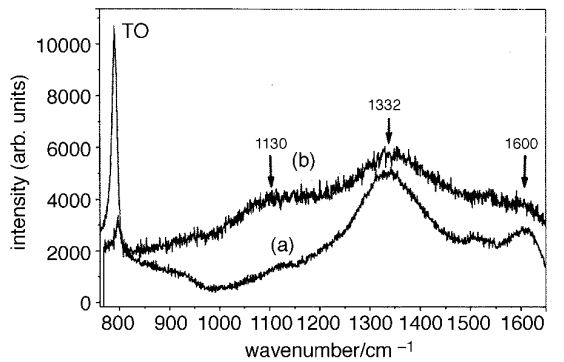

Fig. 10 Typical Raman spectra (excitation line 632.8 nm) of β-SiC powders treated in (a) Ar–2% Cl_2–2% H_2 at 1000 °C for 72 h and (b) Ar–2.4% Cl_2–1.5% H_2 at 950 °C for 72 h

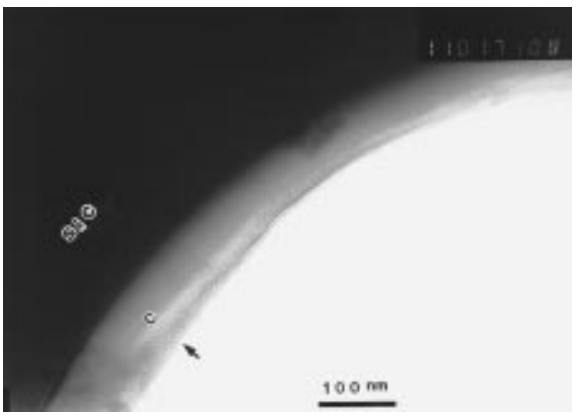

Fig. 11 Bright field TEM micrograph showing the carbon film on a β-SiC particle treated in Ar–3.5% Cl_2 at 600 °C for 27 h

TEM. Numerous carbon particles and graphitic carbon films on the surface of SiC particles have been found in the sample treated with 3.5% Cl_2–Ar at 600 °C as shown in Fig. 11. At the same time, the presence of filamentous carbon and graphite whiskers (Fig. 12) demonstrates the importance of carbon transport *via* the gas phase. Some of the whiskers show ring diffractions that may be ascribed to amorphous silica. Thus, those may be silica whiskers covered with a carbon film. The thicker and highly oriented graphite films, as shown in Fig. 13, were detected in the sample that was treated under similar conditions at 1000°C. The TEM micrographs show that as the temperature increases, thicker and more highly ordered carbon

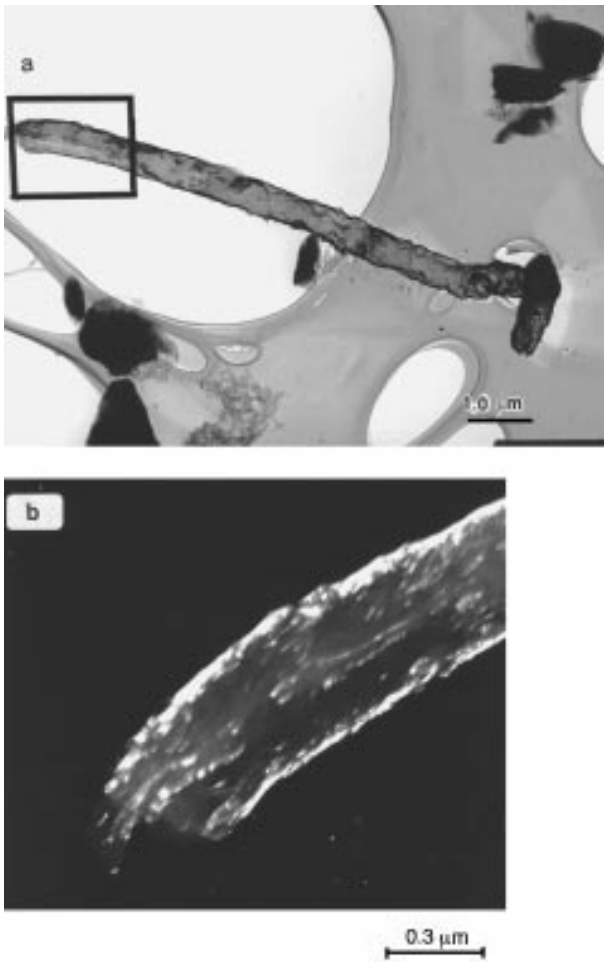

Fig. 12 (a) Bright field TEM micrograph of a whisker in a β-SiC particle treated in Ar–3.5% Cl_2 at 600 °C for 27 h and (b) a dark field micrograph of the whisker top showing the texture of graphite

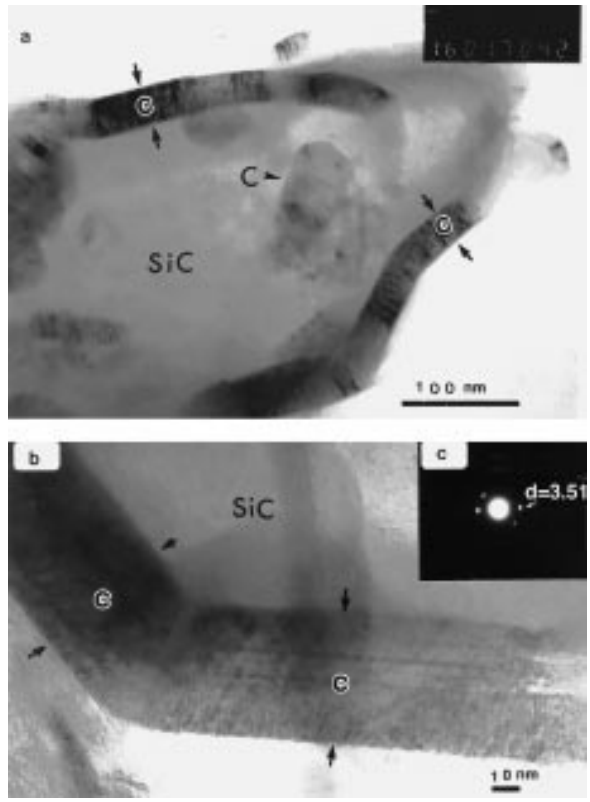

Fig. 13 Representative bright field TEM micrographs showing graphite coating on β-SiC particles after treatment in Ar–3.5% Cl_2 at 1000 °C for 20 h (a,b) and a typical SAD pattern (c)

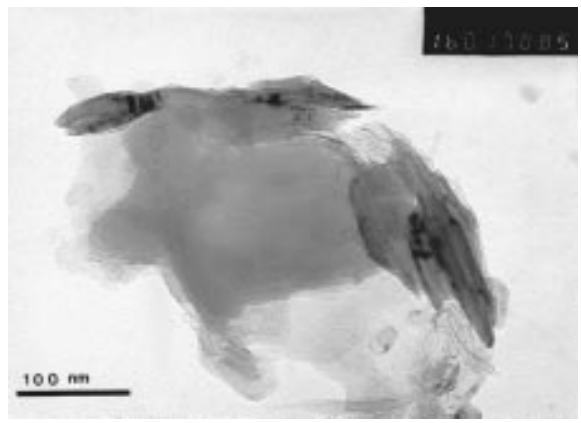

Fig. 14 A typical bright field TEM micrograph of β-SiC treated in Ar–2% Cl_2–2% H_2 at 1000 °C for 72 h

films grow due to reaction with the Cl_2 atmosphere. These films produce diffraction patterns of graphite [Fig. 13(c)].

Uniform carbon films were rarely present on the surface of β-SiC particles treated with 2% Cl_2–2% H_2 at 1000 °C. The amount of carbon was small and β-SiC was the main constituent. Selected area diffraction (SAD) patterns show reflections at $d = 0.206$ nm in carbon-containing regions (Fig. 14). These can be ascribed to diamond. However, no well shaped diamond particles were found. This confirms that the broad bands in the diamond region, which were observed in Raman analyses, could arise from nanocrystalline diamond.

BET. Results of BET specific surface area measurements are shown in Table 1. It can be seen that the powder treated at 1000 °C in Cl_2 has a specific surface area of about 1000 $m^2\ g^{-1}$. This value is typical for active carbons.[23] Other experiments with Cl_2 produced powders with surface areas of 100–200 $m^2\ g^{-1}$. However, these powders contained various amounts of non-reacted SiC. To determine the carbon content in the powders, the samples treated with the Cl_2 gas were oxidized in air in the temperature range from room temperature to 750 °C and the mass changes were measured by TG. The results (Table 1) show that the surface area increases with the increasing carbon content. Based on the SEM and TEM observations, we assume that the treatments did not change the shape of SiC particles and, respectively, did not affect the surface area of SiC nuclei. Thus, the observed increase in the specific surface was in all cases due to carbon coatings formed on SiC. Using the measured specific surface of powders and carbon content we calculated the specific surface of carbon as follows

$$S_c = [S - (S_{SiC})(100\ \text{mass\%C})]/\text{mass\%C} \quad (9)$$

where S is the measured specific surface area of the powder, S_{SiC} is the specific surface area of as-received SiC powder and mass% C is the carbon content in the powder.

We found that all porous carbon coatings on SiC particles have a high surface area, but the surface area increases with increasing time and/or temperature of the treatment in Cl_2 (Table 1).

Treatments in Cl_2–H_2 atmospheres did not increase the surface area of the powder. Still, small amounts of carbon were formed in agreement with thermodynamic calculations as confirmed by Raman analysis and TEM. A low surface area

in the latter case led us to the conclusion that a different structure of the carbon was formed after treatment in Cl_2–H_2.

Discussion

We can divide all experiments into two groups: Cl_2 treatment and Cl_2–H_2 treatment.

Interaction with Cl_2

In the first group of experiments (Cl_2 environment), large amounts of carbon were formed as indicated by EDS and Raman spectra in accord with the results of our thermodynamic calculations and previous reports.[6,8,13] This was amorphous carbon or nanocrystalline graphite film as shown by XRD, Raman spectroscopy and TEM. As the temperature increased, the thickness of the carbon films increased as shown in the TEM micrographs (Fig. 11 and 13).

In the XRD analysis, the condensed carbon phases were not detected probably owing to their amorphous or nanocrystalline state. Graphite or diamond must have a crystal size of above 10 nm and be present in a quantity of several percent to show an XRD pattern. The calculated size of graphite crystallites in our experiments is <5 nm (Table 1).

At 800–1000 °C, the carbon formed from Cl_2 treatments has a surface area of $>1000\ m^2\ g^{-1}$. The specific surface area of $1000\ m^2\ g^{-1}$ is close to the maximum surface area of carbon, since the calculated surface area for an extended graphite layer plane, counting both sides, is about $2800\ m^2\ g^{-1}$.[23] Taking into account the measured specific surface area and TEM observations (Fig. 11,13), which do not reveal the porosity in carbon films even at $>350\,000\times$ magnification, we can assume that the pore size is <1 nm. According to the classification scheme outlined in ref. 23, this is a microporous carbon (although the term 'subnanoporous' would be more exact). Carbon with a comparable surface area and pore size can be obtained, for instance, by steam activation of anthracite.[23] More detailed consideration of the pore structure of carbon films is outside the scope of this paper.

It is important to note that the formation of carbon is very uniform (Fig. 13) and does not change the shape of SiC particles. This suggests the growth of carbon by extraction of Si from SiC and collapse of the cubic structure of β-SiC to amorphous carbon. However, small amounts of carbon found on the surface of uniform transformed layers could be deposited from the gas phase *via* such reactions as:

$$CCl_4\ (g) = C\ (s) + 2\ Cl_2\ (g) \quad (10)$$

$$CO\ (g) = C\ (s) + 1/2\ O_2\ (g) \quad (11)$$

Interaction with Cl_2–H_2 mixtures

In the treatment with Cl_2–H_2 gas mixtures, a very low graphitization degree and size of graphite crystallites were observed (see Table 1). Calculations using eqn. (8) show that if the spectra shown in Fig. 10 (a) and (b) were ascribed to graphite, the calculated grain size (*ca.* 0.4 nm) would approach the unit-cell size ($a = 0.24$ nm) of graphite. Thus, the above spectra should be due to the presence of disordered diamond (or its mixture with sp^2 carbon) rather than graphite. Similar spectra were obtained from nanocrystalline diamond powders.[24] By the thermodynamic calculation (Fig. 3), the amount of carbon should not be much smaller than that formed in a pure Cl_2 atmosphere (Fig. 2) and should increase linearly as the $Cl_2 : H_2$ ratio increases. In these experiments much less carbon was formed in the Cl_2–H_2 atmospheres compared to Cl_2 treatment. In the case of 2% Cl_2–2% H_2 treatment at 1000 °C, the presence of crystalline diamond was confirmed by TEM. Considering that this powder shows only a broad Raman band in the diamond region as shown in Fig. 7, the presence of diamond in other samples treated in Cl_2–H_2 showing similar Raman spectra is likely as well. Fig. 7 shows rather sharp peaks at *ca.* $1330\ cm^{-1}$, which can arise from diamond. However, the simultaneous presence of graphite peaks makes it difficult to distinguish between the Raman band of disordered diamond and the D band of graphite and so the identification of diamond in these samples is not unambiguous. Since diamond was not detected in XRD analysis, it is likely that nanocrystalline diamond was present in very small quantities.

From the thermodynamic calculations it is expected that carbon film formation on β-SiC will occur upon etching in Cl_2 or Cl_2–H_2 mixture gases, and this was confirmed experimentally. The thermodynamic calculations do not distinguish between the conditions for amorphous sp^2 carbon and for diamond or sp^3 carbon. However, in our experiments diamond or sp^3 carbon formed only when hydrogen–chlorine mixture gases were used. The thermodynamic calculations do not predict that the amount of carbon formed in the reaction with Cl_2–H_2 is much less than that in pure Cl_2 above *ca.* 700 °C. However, in our experiments the difference was very significant as shown in all analyses. This may be because experiments performed in an open system permitted gasification of graphitic carbon due to its interaction with hydrogen. It is known that hydrogen plays an important role in diamond synthesis independent of the method. It was reported that sp^3-C is formed on the β-SiC by hydrogen ion etching.[26] In our experiment, sp^3-C is formed in the treatment with the 2% Cl_2–2% H_2 and the 2.6% Cl_2–1.3% H_2 mixtures.

The formation of diamond can occur by two possible mechanisms. One is extraction of carbon from the structure of β-SiC, stabilization of dangling bonds of carbon with hydrogen and further desorption of hydrogen with the formation of diamond. Molecular dynamics calculation[25] shows that helium-filled silicon vacancies are energetically more stable as compared to unoccupied vacancies. The effect of hydrogen in stabilization of Si vacancies and thus the cubic structure of β-SiC when Si is extracted, is assumed to be the same. The above calculations showed that a Si atom can be spontaneously replaced by a carbon atom from the energy point of view. This shows how the SiC structure can be transformed into diamond. However, only very thin films or small particles can be formed this way due to obvious diffusion barriers through the growing diamond. Another possible mechanism is the deposition of diamond from the gas phase by decomposition of $CCl_4(g)$ or $CH_4(g)$ formed by reactions (1) and (7).

Such reactions, as for instance, eqn. (10) and (11) and

$$CH_4\ (g) = C\ (s) + 2\ H_2\ (g) \quad (12)$$

or

$$CCl_4\ (g) + 2\ H_2\ (g) = C\ (s) + 4HCl\ (g) \quad (13)$$

can result in diamond growth on the surface of SiC. Silicon carbide is widely used as a substrate for diamond depositions[27] because of a partial matching between the diamond lattice ($Fd3m$ space group) and the β-SiC lattice ($F\bar{4}3m$ space group). The first mechanism can lead to diamond nucleation and the latter to its further growth.

This route to diamond growth is not surprising in view of the fact that first experiments on diamond growth by thermal decomposition of CBr_4 and CI_4 at 900 °C were conducted 40 years ago.[28] The importance of the use of initial carbon-containing molecules with sp^3-bonding (as in the case of SiC) was stressed by Spitsyn.[29] The major difference in our case is that we used SiC as a substrate and source of carbon simultaneously.

Potential applications

Carbon films find numerous applications in a wide range of fields. Although more detailed studies of the properties of

carbon films obtained on the surface of SiC may be necessary, we can suggest the following potential applications.

1. Weak carbon coatings on SiC fibers, whiskers and platelets can gradually improve the fracture toughness and work of fracture of ceramic matrix composites.[28] Treatments in Cl_2 can be used to obtain coatings on any SiC reinforcement for composites.

2. Active carbon coatings on carbides may be of interest for catalysis and/or medical applications. Carbon materials with a high surface area are ideal as catalyst supports. Since the degree of porosity can be controlled by parameters of the treatment, materials with a specific adsorption capacity can be provided. Additionally, thin films of active carbon can be obtained on SiC fibers or fabrics, allowing the use of special shapes that cannot be obtained from natural carbons.

3. Since reduction of the SiC surface is possible, powders with improved sinterability may be obtained. About 0.5% of free carbon is usually added to SiC to enable its pressureless sintering. A uniform distribution of such a small amount of carbon is difficult, since any large inclusions can cause flaw formation and decrease in mechanical properties. Chlorination of SiC powders can produce very thin and uniform films that should be perfect for improving the sinterability.

4. The formation of diamond shows that if any activation method is used (plasma, hot wire or other technique), synthesis of diamond films on the surface of SiC should be possible without any carbon supply from the gas phase. This can be used as an alternative to CVD diamond synthesis or as a method of obtaining intermediate thin diamond (sp^3-carbon) films for further CVD deposition of diamond on the surface of SiC and other carbides.

5. Both graphitic and diamond films are used in tribology to decrease coefficients of friction and improve wear resistance of sliding parts. A new methods of covering carbides with carbon films may be of practical importance for ceramic bearings and other tribological applications.

Conclusions

1. The formation of carbon upon interaction of silicon carbide with Cl_2 and Cl_2–H_2 gases was predicted. Carbon yield has a maximum in Cl_2–H_2 mixtures which shifts to higher temperatures with increasing pressure.

2. Uniform amorphous carbon or nanocrystalline graphite films were produced by the reaction of the β-SiC powder with chlorine gas at temperatures of 600–1000 °C and at atmospheric pressure. As temperature increases, the thickness of the film formed after a fixed period of exposure increases. The carbon films have a disordered structure with the surface area $>1000\ m^2\ g^{-1}$ and porosity in the nanometer range. Small amounts of oxygen did not affect the formation of carbon films, but result in the simultaneous formation of amorphous silica.

3. When the hydrogen–chlorine gas mixture was used with an appropriate ratio of Cl_2 and H_2, traces of nano- or microcrystalline diamond were found.

This research was supported by NSF through Grant GMS-9617452. We would like to acknowledge the help of Ms. Bettine Geissler with BET analysis, Mr. Oliver Maute with FTIR spectroscopy, (both are with the University of Tübingen, Germany), and Dr. G. E. Khomenko with TEM (the Institute of Materials Science, Kiev, Ukraine). We appreciate the help of Professor P. Kofstad and Professor A. Olsen who gave us access to TEM instruments at the University of Oslo under a NATO Linkage Grant 940706. We extend our thanks to Professor K. G. Nickel from the University of Tübingen for his support and useful discussion.

References

1 Y. G. Gogotsi and M. Yoshimura, *Nature* (*London*), 1994, **367**, 628.
2 Y. G. Gogotsi, M. Yoshimura, M. Kakihana, Y. Kanno and M. Shibuya, *Ceram. Trans.*, 1995, **51**, 243.
3 Y. G. Gogotsi, in *Korrosion und Verschleiss von keramischen Werkstoffen*, ed. R. Telle and P. Quirmbach, DKG, 1994, p. 114.
4 Y. G. Gogotsi, P. Kofstad, M. Yoshimura and K. G. Nickel, *Diamond Relat. Mater.*, 1996, **5**, 151.
5 Y. G. Gogotsi, K. G. Nickel and P. Kofstad, *J. Mater. Chem.*, 1995, **5**, 2313.
6 M. J. McNallan, S. Y. Ip, S. Y. Lee and C. Park, *Ceram. Trans.*, 1990, **10**, 309.
7 W. S. Pan and A. J. Stekl, *J. Electrochem. Soc.*, 1990, **137**, 212.
8 M. Balooch and D. R. Olander, *Surf. Sci.*, 1992, **126**, 321.
9 K. J. Grannen and R. P. H. Chang, *J. Mater. Res.*, 1994, **9**, 2154.
10 D. Roy, P. Ravindrananthan and A. Badzian, *J. Mater. Res.*, 1996, **5**, 1164.
11 S. Y. Ip, M. J. McNallan and M. E. Schreiner, *Ceram. Trans.*, 1989, **2**, 289.
12 D. S. Park, M. J. McNallan, C. Park and W. W. Liang, *J. Am. Ceram. Soc.*, 1990, **73**, 1323.
13 E. Marra, R. Kreidler, N. S. Jacobson and D. S. Fox, *J. Am. Ceram. Soc.*, 1988, **71**, 1067.
14 M. Gorman and S. A. Solin, *Solid State Commun.*, 1974, **51**, 761.
15 R. J. Nemanich, J. T. Glass, G. Lucovsky and R. E. Shroder, *J. Vac. Sci. Technol. A*, 1988, **6**, 1783.
16 Y. G. Gogotsi, K. G. Nickel, D. Bahloul-Hourlier, T. Merle-Mejean, G. E. Khomenko and K. P. Skjerlie, *J. Mater. Chem.*, 1996, **6**, 595.
17 I. D. Jeon, M. J. McNallan and Y. Gogotsi, *Fundamental Aspects of High Temperature Corrosion VI*, ed. D. A. Shores, R. Rapp and P. Hou, Proceedings of 190th ECS Meeting, San Antonio, TX, Oct. 1996, pp. 256–268.
18 J. E. Marra, E. C. Kreidler, N. S. Jacobson and D. S. Fox, *J. Electrochem. Soc.*, 1988, **135**, 1571.
19 S. Knight and W. B. White, *J. Mater. Res.*, 1989, **4**, 385.
20 F. Tuinstra and J. L. Koenig, *J. Chem. Phys.*, 1970, **53**, 1126.
21 V. D. Andreev, T. A. Nachalnaya and E. V. Gabrusenok, *Sverkhtverd. Mater.*, 1993, **2**, 11 (in Russian).
22 H. Eto, Y. Tamon, Y. Ohsawa and N. Kikuchi, *Diamond Relat. Mater.*, 1994, **1**, 373.
23 V. McEnaney and T. Y. Mays, *Introduction to Carbon Science*, ed. H. Marsh, Butterworths, 1989, pp. 154–196.
24 E. D. Obraztsova, in *Nanophase Materials*, ed. G. C. Hadjipanayis and R. W. Siegel, Kluwer, Dortmund 1994, pp. 483–492.
25 H. Huang and N. Ghoniem, *J. Nucl. Mater.*, 1994, **212–215**, 148.
26 J. M. Lannon Jr., J. S. Gold and C. D. Stinespring, *J. Appl. Phys.*, 1995, **77**, 3823.
27 W. Yarbrough, *J. Am. Ceram. Soc.*, 1992, **75**, 3179.
28 B. V. Spitsyn and B. V. Deryagin, Authors certificate SU 339134, *A Technique of Diamond Growth on Diamond's Face*, 1956.
29 B. V. Spitsyn, in *Handbook of Crystal Growth*, ed. D. T. J. Hurle, Elsevier, Amsterdam, 1994, pp. 401–456.
30 R. H. Jones, C. H. Schilling and L. H. Schoenlein, *Mater. Sci. Forum*, 1989, **46**, 277–308.

Paper 7/01126A; *Received* 18*th February*, 1997